Femtosecond Dynamics of Fast Electron Pulses in Relativistic Laser-Foil Interactions

Guoqian Liao [1,2,6,*] Fangzheng Sun,[1,2] Hongyi Lei [1,2] Tianze Wang,[1] Dan Wang,[1] Yanyu Wei,[1,2]
Feng Liu,[3,4] Xuan Wang,[1,6] Yutong Li,[1,2,4,6,†] and Jie Zhang [1,3,4,5]

[1]*Beijing National Laboratory for Condensed Matter Physics, Institute of Physics, Chinese Academy of Sciences, Beijing 100190, China*
[2]*School of Physical Sciences, University of Chinese Academy of Sciences, Beijing 100049, China*
[3]*Key Laboratory for Laser Plasmas (Ministry of Education), School of Physics and Astronomy,
Shanghai Jiao Tong University, Shanghai 200240, China*
[4]*Collaborative Innovation Center of IFSA (CICIFSA), Shanghai Jiao Tong University, Shanghai 200240, China*
[5]*Tsung-Dao Lee Institute, Shanghai 200240, China*
[6]*Songshan Lake Materials Laboratory, Dongguan, Guangdong 523808, China*

We report the femtosecond time-resolved dynamics of relativistic electron pulses in ultraintense laser-foil interactions, by characterizing the terahertz self-radiation with single-shot ultrabroadband interferometry. Experimental measurements together with theoretical modeling reveal that the electron pulses inherit the duration of the driving laser pulse. We also visualize the electron recirculation dynamics, where electrons remain trapped inside the self-generated electrostatic potential well and rebound back and forth around the thin foil for hundreds of femtoseconds. Our results not only demonstrate an *in situ*, real-time metrology scheme for electron bursts, but also have important implications for understanding and manipulating the time-domain properties of laser-driven particle and radiation sources.

DOI: 10.1103/PhysRevLett.132.155001

In multiterawatt laser interactions with dense matter, large numbers of electrons on the surface are accelerated to high energies over a tiny spatiotemporal scale, launching a huge current of energetic electrons (termed hereafter as "fast electrons") [1]. Fast electrons have been identified as an essential core underpinning many applications that have attracted tremendous attention, such as, to name just a few, the generation of radiation sources at different frequency bands from microwaves [2] to x rays [3], the sheath acceleration of ion beams [4], the rapid isochoric heating of matter [5], and the fast ignition approach for inertial fusion energy [6]. Fundamentally, the properties of those secondary photon and particle sources as well as the newly created states of matter are deeply related to fast electrons' temporal, spatial, and energy characteristics. Although a lot of studies have been conducted on the fast-electron generation and transport, previous studies mainly focus on the dimensionality in energetics (flux [7], temperature [8]) and spatial morphology (divergence [9], filamentation [10]), with very little knowledge of the time-domain information of fast electrons. From a practical viewpoint, the temporal characteristics and evolution of fast electrons directly determine the emission duration of the resultant x rays and ion beams, as well as the course and efficiency of energy transfer into matter. For example, a unique feature of ultraintense laser-foil interactions is the so-called "recirculation" process, where a large number of fast electrons remain trapped inside the self-generated electrostatic sheath potential well that is built up at the vicinity of thin foils [11]. It has been recognized to play a key role in the enhanced laser absorption [12], ion acceleration [13], secondary radiation [14,15], and bulk heating [16]. However, direct observation of this important process is not yet accessible. Some attempts have been made on the fast-electron evolution dynamics, for example, using optical reflectometry [17,18], interferometry [19], or proton deflectometry [20]; measuring the secondary x-ray [21] or optical emission [22,23]; or detecting the Coulomb fields of electrons that escape the target [24,25]. At best, these measurements have only subpicosecond temporal resolution, and the majority of these approaches require multiple-shot measurements. Hence, unambiguously measuring the femtosecond-scale temporal dynamics of fast electrons *per se* has long been a formidable challenge, which is still a major missing link in understanding the related physics.

In this Letter, we directly map the temporal characteristics and evolution of fast electrons to the terahertz (THz) self-radiation induced when the huge-current electron pulses cross the target surface [26]. Real-time measurements are achieved by utilizing our newly developed single-shot ultrabroadband THz interferometry [27]. We find that the fast-electron bunch duration is comparable to the laser pulse width, and reveal the fast-electron femtosecond-scale recirculation dynamics in the time domain.

The experiment (Fig. 1 and Supplemental Material, Fig. S1) was performed with the multiterawatt Ti:sapphire laser system at the Laboratory for Laser Plasmas, Shanghai
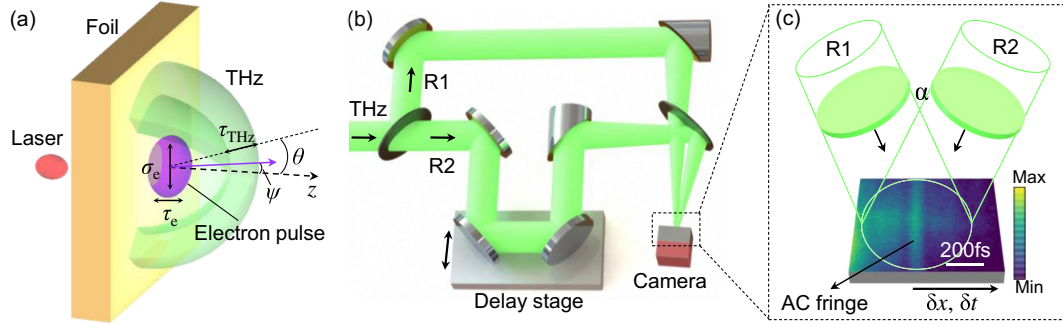
FIG. 1. (a) Schematic illustrating intense laser-foil interactions and the generation of THz radiation by fast electrons traversing the foil's rear surface. (b) Sketch of the noncollinear autocorrelator used for single-shot ultrabroadband THz detection. The collimated THz radiation is split into two replica beams (R1 and R2) with a beam splitter. After appropriate optical path delay, the two beams are focused and recombined noncollinearly at a cross angle of α onto the THz camera. (c) Schematic showing the noncollinear AC-based detection principle and a typical AC interferogram. The noncollinear geometry provides the space-to-time mapping between the spatial position, δx, in the THz spot and the relative time delay, δt, of the two replica beams as $\delta t = 2\delta x \cdot \sin(\alpha/2)/c$, where c is the light velocity in vacuum.

Jiao Tong University. *P*-polarized laser pulses of adjustable durations were focused onto a foil target at an incidence angle of ∼30°, creating a peak intensity of ∼3 × 10^{19} W/cm² with the 35-fs full-width-at-half-maximum (FWHM) duration. No sign was observed that the laser pulse penetrated through the thin foil or the target rear surface was damaged during laser interactions. The laser-accelerated fast electrons transported through the target, and self-consistently produced strong THz radiation primarily via the coherent transition radiation (CTR) process when crossing the metallic rear surface [26,28]. A single-shot electro-optic (EO) detection scheme was tried to measure the THz waveform [27], showing subcycle Gaussian-like temporal profiles with a relatively constant duration at ∼200 fs (see Supplemental Material, Fig. S2). This is because of the finite detectable bandwidth and temporal resolution of EO measurements. On one hand, the EO crystals usually have a limited response bandwidth that may not be able to cover the whole THz spectrum to be measured. On the other hand, the laser probe available in most ultraintense laser systems has a finite duration (∼35 fs in our experiment), which cannot directly provide time resolution high enough to accurately measure the tens-of-femtosecond THz pulses. To crack this bottleneck, a novel THz interferometer termed as "noncollinear autocorrelator" [27] was developed without the need of EO crystals and ultrafast laser probes to characterize the THz radiation. The autocorrelation (AC) of beam-division THz pulses at a noncollinear configuration enables single-shot ultrabroadband measurements of the THz AC interferogram [Figs. 1(b) and 1(c)]. Calibrations showed that the space-time mapping relationship, $\delta t/\delta x$, was ∼8.3 fs/pixel. Meanwhile, an imaging diagnostic for the optical transition radiation (OTR) [23] near the target rear normal was fielded to monitor the transverse profile of fast electrons, showing that the fast electrons transported approximately at a constant divergence angle with an initial size comparable to the

laser focal spot size. Wraparound image plate stacks and an electron spectrometer were used in some shots to evaluate the angular distribution and temperature of escaping electrons, respectively. Measurements showed that the electrons were ejected primarily around $\psi \sim 16°$ with respect to the target rear normal, and the electron temperature, T_e, was positively correlated to the laser intensity. More details on the experimental diagnostics and data can be found in the Supplemental Material [29].

First, we study the fast-electron bunch duration as a function of the laser pulse duration, by varying the laser duration incrementally while keeping the intensity at ∼10^{19} W/cm². To avoid the possible interference from electrostatic sheath fields formed at the target rear surface, double-layered targets consisting of a copper (Cu) foil backed by a 100-μm thick plastic (CH) layer (referred to hereafter as Cu-CH targets) are employed. A subcycle THz pulse will be induced via the CTR process by fast electrons crossing the Cu-CH interface [26]. The measured THz AC interferogram is rendered as a clear fringe on the THz spot [see Fig. 1(c)]. Figure 2(a) shows a typical AC signal extracted experimentally, indicating an approximately Gaussian-shaped trace. Its Fourier transform directly yields the THz spectrum. Since the CTR pulse has a quasi-half-cycle waveform [see Fig. 2(c)] and EO measurements show that the THz waveform is approximately Gaussian shaped (see Supplemental Material [29], Fig. S2), the THz duration is correlated to the THz spectrum, and can therefore be inferred from the AC measurements (see Supplemental Material [29], Table S1). Measurements show that the THz duration broadens with increasing laser duration [Fig. 2(b)]. Interestingly, for short laser durations, the THz duration is a little greater than the corresponding laser duration, while for long laser durations, the THz duration becomes smaller than the laser duration.

To retrieve the fast-electron bunch duration from the THz duration, it is imperative to establish the mapping
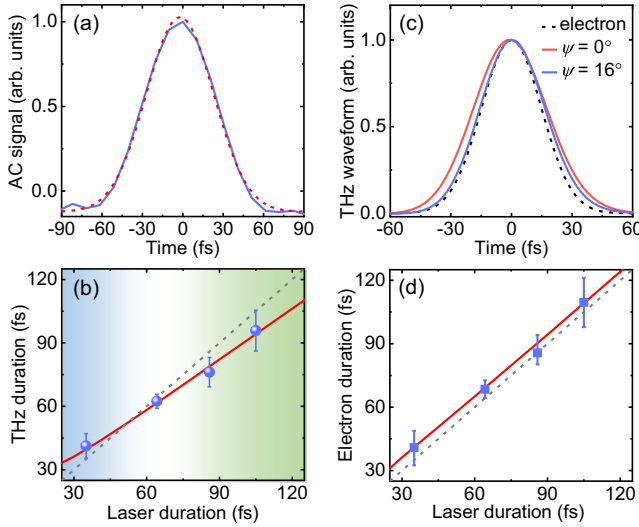
FIG. 2. Retrieval of fast-electron bunch durations. (a) A typical THz AC trace measured at the Cu-CH targets (where the Cu-layer thickness is 10 μm) impinged upon by 35-fs laser pulses, and fit with a Gaussian function (dashed red). (b) Experimentally measured (blue dots) and numerically calculated (red curve) THz duration as a function of the laser pulse duration. (c) Normalized THz CTR waveforms ($\theta = 36°$) calculated for an electron bunch ($\tau_e = 35$ fs, $\sigma_e = 11$ μm, and $T_e = 0.8$ MeV) leaving perpendicularly (red, $\psi = 0°$) or obliquely (blue, $\psi = 16°$) to a metal-vacuum interface. The black dashed curve denotes the original Gaussian electron bunch waveform with a duration of 35 fs. (d) Experimentally retrieved electron bunch duration (blue squares) versus the laser pulse duration and the comparison with numerical calculations (red curve). The dashed diagonal in (b) and (d) represents the duration being equal to the laser duration, and the error bars are estimated based on the shot-to-shot fluctuation and the fitting uncertainty of the experimental AC traces.

relationship between the fast-electron characteristics and THz properties. Owing to the fact that fast electron bunch is divergent, the electron bunch gradually grows in transverse size during transport. The resulting THz radiation is the coherent superposition of the fields produced by electrons at different spatiotemporal positions, i.e., as a result of the convolution of spatiotemporal properties of fast electrons. Specifically, for an electron bunch with a Gaussian-like spatiotemporal distribution, the THz duration, τ_{THz}, is dependent largely on the spatiotemporal parameters of electron bunches given by (see Supplemental Material [29])

$$\tau_{THz}^2 \approx (\tau_e \delta)^2 + (\sigma_e \sin \theta / c)^2, \tag{1}$$

where τ_e and σ_e are the electron bunch duration and transverse size, respectively, $\delta = 1 - \beta \sin \theta \sin \psi$ is the modification factor of Doppler frequency shift due to the oblique ejection of electrons, θ and ψ are the observation angle and the electron ejection angle with respect to the interface normal, respectively, and β is the electron velocity

normalized by the light velocity in vacuum, c. Equation (1) indicates that, besides the temporal (longitudinal) structure, the spatial (transverse) profile and ejection configuration of electrons also contribute to the THz duration, which is not well established in theory previously [30]. More specifically, the finite transverse spread of electrons will broaden the resultant THz duration [red curve in Fig. 2(c)], while the oblique ejection of electrons will reduce the THz duration [blue curve in Fig. 2(c)].

According to Eq. (1) and the experimentally measured spatial profile of electrons ($\sigma_e \sim 11$ μm and $\psi \sim 16°$), one can retrieve the bunch duration of the fast electrons ejected at the Cu-CH interface [Fig. 2(d)], which is shown to be only several femtoseconds greater than the laser duration. Such a small broadening probably comes from the velocity dispersion during fast-electron transport. To check this, numerical calculations of the electron transport and THz generation are performed (see Supplemental Material [29]) on the premise that the fast electrons initially inherit the duration of the laser pulse, and transport through the 10-μm-thick copper at a constant divergence angle. The calculated THz and electron durations are in good accordance with the experimental measurements [see red curves in Figs. 2(b) and 2(d)]. To the best of our knowledge, this is the first accurate measurement of femtosecond fast-electron bunch durations in laser-solid interactions, validating that the ultraintense laser-accelerated electron beam has a temporal envelope comparable to the driving laser pulse.

We now look into the temporal evolution of electrons during transport and the influence of the self-generated sheath fields, by comparing the THz radiation emitted from the Cu foils and Cu-CH targets as a function of the Cu-layer thickness (Fig. 3). The measured THz AC interferograms broaden incrementally, and the evaluated THz duration augments gradually from ~40 fs to ~100 fs. According to Eq. (1), it reflects the broadening of the electron envelope both longitudinally and transversely during transport. Numerically calculated results [red curves in Figs. 3(a) and 3(b)] agree well with the experimental measurements except for the 5-μm- and 10-μm-thick Cu foils.

A distinct feature appears in the THz AC traces for the 5-μm- and 10-μm-thick Cu foils, manifested as two symmetric delayed satellite peaks beside the main peak [marked with arrows in Fig. 3(c)], implying double pulses generated in the THz waveform. Since the sheath field is suppressed greatly at the Cu-CH interface but not for the Cu foil target, we believe that such different THz characteristics stem from the distinct electron dynamics governed by strong sheath fields at the Cu foil surface. When some electrons escape from the thin target, a strong electrostatic sheath field is built up at the rear surface [4]. This field reflects subsequent low-energy electrons back into the target, as illustrated in Fig. 3(d). This rebound process is commonly called "recirculation" [11]. For our experimental configurations, the ~90-fs dwell time [31] of the laser
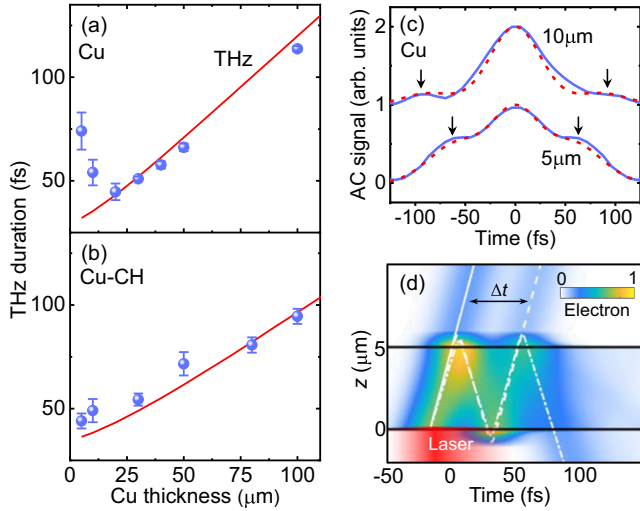
FIG. 3.   Experimentally measured (blue dots) and numerically calculated (red curves) THz durations as a function of the Cu-layer thickness for (a) Cu foils and (b) Cu-CH targets. Recirculation is not considered in the calculations. The error bars are estimated based on the shot-to-shot fluctuation and the fitting uncertainty of the experimental AC traces. (c) THz AC traces (blue solid) measured at 5-μm and 10-μm Cu foils, and a comparison with numerical calculations taking recirculation into account (red dashed). (d) Spatiotemporal evolution of electrons illustrating the laser reacceleration of refluxing electrons, leading to the ejection of two electron pulses and accordingly the generation of dual-pulse THz radiation. The white curves represent the traces of electrons at different energies (solid, 1.6 MeV; dashed, 0.8 MeV; dash dotted, 0.4 MeV). See the Supplemental Material [29] for more details on the modeling of recirculation.

pulse on the target front surface is longer than twice of the transit time of electrons through the 5-μm- and 10-μm-thick foils, and the refluxing electrons returning to the front surface will be reaccelerated back into the target by the intense laser field that still exists at the front surface, leading to the ejection of the second electron pulse from the rear surface and thus inducing dual-pulse THz radiation. This agrees well with the experimental observation. From the measured THz AC interferograms, one can infer characteristic parameters of refluxing dynamics including the time delay, Δt, and the flux ratio, R_e, of the second electron pulse to the first one. For the 5-μm foil, $\Delta t \sim 60$ fs and $R_e \sim 1$, while for the 10-μm foil, $\Delta t \sim 95$ fs and $R_e \sim 0.15$. If roughly assuming that the dwell time of electrons in the sheath fields at the rear surface and laser fields at the front surface does not change for the 5-μm- and 10-μm-thick foils, one can infer the average velocity of refluxing electrons in the target to be approximately $\sim 10 \ \mu m/(95-60)$ fs $= 0.95c$, corresponding to an average kinetic energy of ~ 1.1 MeV. When the foil thickness increases from 5 μm to 10 μm, the significant drop of R_e suggests that the number of electrons returning to the laser focal area and reaccelerated into the target by the laser

fields decreases dramatically, due to the large angular divergence of fast electrons.

To further investigate the electron recirculation dynamics, a plasma mirror is employed in the experiment to substantially boost the laser contrast, allowing for the production of strong sheath fields at the target front surface after the laser pulse turns off. As illustrated in Figs. 4(a) and 4(b), under the synergistic action of strong sheath fields at both the front and rear target surfaces, most of the electrons will remain trapped inside the sheath potential well, and travel back and forth through the foil for multiple round trips. The deceleration and acceleration of electrons by the sheath fields or their leaving and reentering the target will induce transient emission termed bremsstrahlung-like transition radiation (bTR) (see Supplemental Material [29]) as a special case of transition radiation [32], which usually has a bipolar field waveform [see the red dashed curve in Fig. 4(b)]. As a result, such an electron recirculation process will be featured by a multicycle THz emission.

Figures 4(c)–4(e) show the THz AC interferograms measured with thin Cu foils. Notably, periodic fringe arrays are presented, and the fringe spacing widens with the increase of foil thickness. No such periodic fringes are observed either in the moderate laser contrast case (where there is no strong sheath field at the target front surface) or for the Cu-CH targets (where sheath fields at the Cu rear surface are suppressed greatly). The experimental results convince us that the observed multicycle THz radiation is a specific marker of the electron recirculation through the thin foil back and forth.

The measured THz AC interferograms directly provide the spectral information of multicycle THz radiation. Theoretical modeling (see Supplemental Material [29]) indicates that the recirculation-induced THz radiation has a spectrum peaked approximately at $\omega_c \sim 2\pi/\Delta t_{rec}$ with a bandwidth of $\Delta\omega \sim 2\pi/T_{rec}$, where $T_{rec} \sim N_{rec} \cdot \Delta t_{rec}$ is the recirculation duration, N_{rec} is the recirculation number, and Δt_{rec} is the average time interval between successive recirculation, depending mainly on the foil thickness and the average sheath field strength, E_{sh}. These parameters can be inferred by reproducing the measured THz interferograms and spectra with numerical calculations [see Figs. 4(f)–4(h) and Supplemental Material [29], Fig. S4]. The slight discrepancy between the measured and calculated AC interferograms could be mainly due to the simplified treatment adopted in the calculations where collimated refluxing electrons and uniform constant sheath fields are assumed. E_{sh} is evaluated to be at the TV/m level, and it increases with decreasing target thickness [Fig. 4(i)]. A further comparison of our results with the well-known sheath model of isothermal plasma expansion [34] indicates that the laser-to-electron conversion efficiency, η, is enhanced significantly by electron recirculation [red curves in Fig. 4(i)], in good accordance with previous experiments [12].
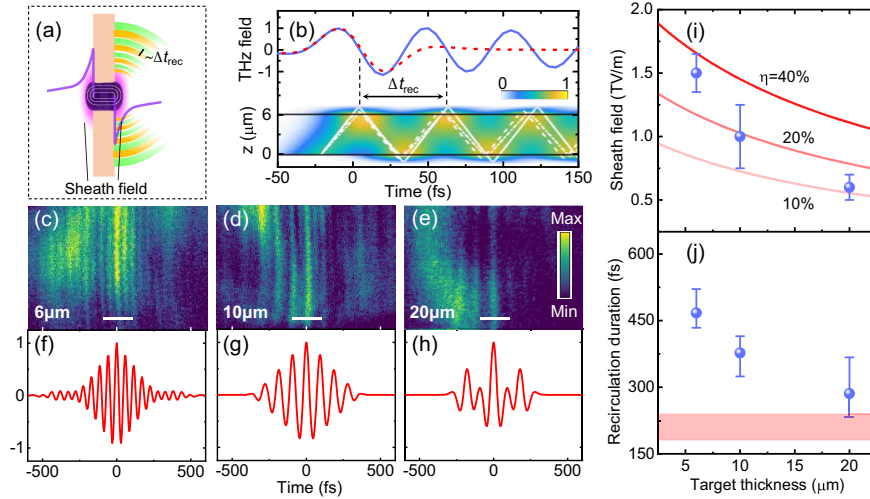
FIG. 4. (a) Schematic illustrating the electron recirculation dynamics and resultant multicycle THz radiation induced at the target rear. (b) Calculated spatiotemporal evolution of electrons (color map) and the resultant THz field waveform (blue curve). The white curves in the color map represent the traces of electrons at different energies (solid, 1.6 MeV; dashed, 0.8 MeV; dash dotted, 0.4 MeV). The red dashed curve denotes the bipolar waveform of bTR induced at the first recirculation. (c)–(e) THz AC interferograms measured for different Cu foil thickness. The nonuniformity of interferograms along the vertical coordinate is due to the imperfect optical alignment or defective THz elements. In the high-contrast laser case, measurements showed that the electrons were ejected primarily around $\psi \sim 0°$, and θ was switched to $\sim 50°$ in order to collect more bTR. The white scale bars represent 200 fs. (f)–(h) Numerically calculated THz AC traces. See the Supplemental Material [29] for the calculation details. (i) Experimentally inferred sheath field strength and (j) recirculation duration. Red curves represent the theoretical projections at the indicated laser-to-electron conversion efficiency, η. The red shaded area shows the ion acceleration time evaluated by the empirical scaling law [33] in which the recirculation is not considered.

Since the electron recirculation and ion acceleration coexist at the target surface, it is reasonable to use the T_{rec} to approximately characterize the ion acceleration time, t_{acc}, an important parameter but difficult to be measured so far [33]. T_{rec} or t_{acc} is inferred to be a few hundred femtoseconds (much longer than the laser duration), and get significantly boosted at thin targets [Fig. 4(j)]. Note that, T_{rec} is much shorter than the collisional relaxation time ($\sim$a few picoseconds) of relativistic electrons in the copper [22], implying that the energy dissipation of refluxing electrons is not dominated by the collision in the target, but by the evolving sheath field and related dynamics such as plasma expansion, ion acceleration, and secondary radiation generation. It should be noted that, within the subpicosecond recirculation duration, the target rear surface remains a sufficiently high density for the THz generation, and the density scale length is much less than the THz wavelength. Hence, it is still a good approximation to model the foil surface as a sharp metallic boundary, i.e., the THz generation will not be affected much by the plasma formation and expansion during the electron recirculation.

In conclusion, by harnessing characterization of the self-induced THz transition radiation with noncollinear autocorrelation-based interferometry, we have made *in situ*, real-time measurements of the femtosecond temporal dynamics of energetic electron pulses produced in ultraintense laser interactions with metal foils. Our results demonstrate that, the intense electron beam at its generation has a comparable duration to the driving laser pulse, and then broadens both temporally and spatially during transport. Under the interplay of the laser pulse and strong sheath fields, some electrons travel back and forth through the thin foil even for a few hundred femtoseconds. To the best of our knowledge, this is the first unambiguous experimental observation in the time domain of the electron recirculation dynamics. The fast-electron metrology demonstrated here will help provide new insights into understanding from the time dimension the complex physics governing the fast-electron generation and transport in solids, and further manipulating the temporal structure and duration of secondary sources (e.g., THz radiation, x rays, and ion beams) as well as the dynamics of energy transfer from electrons to solids. We anticipate that, the single-shot probe-free THz characterization strategy could also be extended to shorter wavelengths (ultraviolet even x rays) and thus noninvasively unraveling faster (attosecond-level) electron dynamics of interest in both ultrafast light-matter interactions and advanced accelerators.

---

*To whom correspondence should be addressed: gqliao@iphy.ac.cn

†To whom correspondence should be addressed: ytli@iphy.ac.cn

[1] W. L. Kruer, *The Physics of Laser Plasma Interactions* (Westview Press, Boulder, CO, 2003).

[2] F. Consoli *et al.*, Laser produced electromagnetic pulses: Generation, detection and mitigation, High Power Laser Sci. Eng. **8**, e22 (2020).

[3] J. D. Kmetec, C. L. Gordon, J. J. Macklin, B. E. Lemoff, G. S. Brown, and S. E. Harris, MeV x-ray generation with a femtosecond laser, Phys. Rev. Lett. **68**, 1527 (1992).

[4] A. Macchi, M. Borghesi, and M. Passoni, Ion acceleration by superintense laser-plasma interaction, Rev. Mod. Phys. **85**, 751 (2013).

[5] A. Saemann, K. Eidmann, I. E. Golovkin, R. C. Mancini, E. Andersson, E. Förster, and K. Witte, Isochoric heating of solid aluminum by ultrashort laser pulses focused on a tamped target, Phys. Rev. Lett. **82**, 4843 (1999).

[6] M. Tabak, J. Hammer, M. E. Glinsky, W. L. Kruer, S. C. Wilks, J. Woodworth, E. M. Campbell, M. D. Perry, and R. J. Mason, Ignition and high gain with ultrapowerful lasers, Phys. Plasmas **1**, 1626 (1994).

[7] Y. Ping, R. Shepherd, B. F. Lasinski, M. Tabak, H. Chen, H. K. Chung *et al.*, Absorption of short laser pulses on solid targets in the ultrarelativistic regime, Phys. Rev. Lett. **100**, 085004 (2008).

[8] T. Kluge, T. Cowan, A. Debus, U. Schramm, K. Zeil, and M. Bussmann, Electron temperature scaling in laser interaction with solids, Phys. Rev. Lett. **107**, 205003 (2011).

[9] J. S. Green, V. M. Ovchinnikov, R. G. Evans, K. U. Akli, H. Azechi, F. N. Beg *et al.*, Effect of laser intensity on fast-electron-beam divergence in solid-density plasmas, Phys. Rev. Lett. **100**, 015003 (2008).

[10] Y. Sentoku, E. d'Humières, L. Romagnani, P. Audebert, and J. Fuchs, Dynamic control over mega-ampere electron currents in metals using ionization-driven resistive magnetic fields, Phys. Rev. Lett. **107**, 135005 (2011).

[11] Y. Sentoku, T. E. Cowan, A. Kemp, and H. Ruhl, High energy proton acceleration in interaction of short laser pulse with dense plasma target, Phys. Plasmas **10**, 2009 (2003).

[12] R. J. Gray, R. Wilson, M. King, S. D. R. Williamson, R. J. Dance, C. Armstrong *et al.*, Enhanced laser-energy coupling to dense plasmas driven by recirculating electron currents, New J. Phys. **20**, 033021 (2018).

[13] A. J. Mackinnon, Y. Sentoku, P. K. Patel, D. W. Price, S. Hatchett, M. H. Key, C. Andersen, R. Snavely, and R. R. Freeman, Enhancement of proton acceleration by hot-electron recirculation in thin foils irradiated by ultra-intense laser pulses, Phys. Rev. Lett. **88**, 215006 (2002).

[14] P. Neumayer, B. Aurand, M. Basko, B. Ecker, P. Gibbon, D. C. Hochhaus *et al.*, The role of hot electron refluxing in laser-generated K-alpha sources, Phys. Plasmas **17**, 103103 (2010).

[15] Z. Jin, H. B. Zhuo, T. Nakazawa, J. H. Shin, S. Wakamatsu, N. Yugami *et al.*, Highly efficient terahertz radiation from a thin foil irradiated by a high-contrast laser pulse, Phys. Rev. E **94**, 033206 (2016).

[16] N. F. Beier, H. Allison, P. Efthimion, K. A. Flippo, L. Gao, S. B. Hansen *et al.*, Homogeneous, micron-scale high-energy-density matter generated by relativistic laser-solid interactions, Phys. Rev. Lett. **129**, 135001 (2022).

[17] P. Antici, J. Fuchs, M. Borghesi, L. Gremillet, T. Grismayer, Y. Sentoku *et al.*, Hot and cold electron dynamics following high-intensity laser matter interaction, Phys. Rev. Lett. **101**, 105004 (2008).

[18] J. S. Green, N. Booth, R. J. Dance, R. J. Gray, D. A. MacLellan, A. Marshall *et al.*, Time-resolved measurements of fast electron recirculation for relativistically intense femtosecond scale laser-plasma interactions, Sci. Rep. **8**, 4525 (2018).

[19] O. Jäckel, J. Polz, S. M. Pfotenhauer, H.-P. Schlenvoigt, H. Schwoerer, and M. C. Kaluza, All-optical measurement of the hot electron sheath driving laser ion acceleration from thin foils, New J. Phys. **12**, 103027 (2010).

[20] L. Romagnani, J. Fuchs, M. Borghesi, P. Antici, P. Audebert, F. Ceccherini *et al.*, Dynamics of electric fields driving the laser acceleration of multi-MeV protons, Phys. Rev. Lett. **95**, 195001 (2005).

[21] P. M. Nilson, J. R. Davies, W. Theobald, P. A. Jaanimagi, C. Mileham, R. K. Jungquist *et al.*, Time-resolved measurements of hot-electron equilibration dynamics in high-intensity laser interactions with thin-foil solid targets, Phys. Rev. Lett. **108**, 085002 (2012).

[22] M. Shaikh, A. D. Lad, K. Pepitone, J. Jha, D. Sarkar *et al.*, Mapping the damping dynamics of mega-ampere electron pulses inside a solid, Phys. Rev. Lett. **120**, 065001 (2018).

[23] J. J. Santos, F. Amiranoff, S. D. Baton, L. Gremillet, M. Koenig, E. Martinolli *et al.*, Fast electron transport in ultraintense laser pulse interaction with solid targets by rear-side self-radiation diagnostics, Phys. Rev. Lett. **89**, 025001 (2002).

[24] S. Inoue, S. Tokita, K. Otani, M. Hashida, M. Hata, H. Sakagami, T. Taguchi, and S. Sakabe, Autocorrelation measurement of fast electron pulses emitted through the interaction of femtosecond laser pulses with a solid target, Phys. Rev. Lett. **109**, 185001 (2012).

[25] R. Pompili, M. P. Anania, F. Bisesto, M. Botton, M. Castellano, E. Chiadroni *et al.*, Femtosecond dynamics of energetic electrons in high intensity laser-matter interactions, Sci. Rep. **6**, 35000 (2016).

[26] G.-Q. Liao, Y.-T. Li, Y.-H. Zhang, H. Liu, X.-L. Ge, S. Yang *et al.*, Demonstration of coherent terahertz transition radiation from relativistic laser-solid interactions, Phys. Rev. Lett. **116**, 205003 (2016).

[27] F. Z. Sun, G. Q. Liao, H. Y. Lei, T. Z. Wang, Y. Y. Wei, D. Wang, H. Chen, F. Liu, Y. T. Li, and J. Zhang,

A non-collinear autocorrelator for single-shot characterization of ultrabroadband terahertz pulses, Rev. Sci. Instrum. **93,** 123003 (2022).

[28] J. Déchard, X. Davoine, L. Gremillet, and L. Bergé, Terahertz emission from submicron solid targets irradiated by ultraintense femtosecond laser pulses, Phys. Plasmas **27,** 093105 (2020).

[29] See Supplemental Material at http://link.aps.org/supplemental/10.1103/PhysRevLett.132.155001 for details on the theoretical modeling, numerical calculations, experimental diagnostics, and data.

[30] C. B. Schroeder, E. Esarey, J. van Tilborg, and W. P. Leemans, Theory of coherent transition radiation generated at a plasma-vacuum interface, Phys. Rev. E **69,** 016501 (2004).

[31] The laser dwell time on the surface $T_L \approx 2\tau_L + 2\sigma_L \sin\theta_i/c = 90$ fs, where $\tau_L = 35$ fs is the laser duration, $\sigma_L \sim 6$ µm is the laser spot size, and $\theta_i = 30°$ is the laser incidence angle. T_L will be longer if the finite underdense plasmas at the surface are considered.

[32] G.-Q. Liao, H. Liu, G. G. Scott, Y.-H. Zhang, B.-J. Zhu, Z. Zhang *et al.*, Towards terawatt-scale spectrally tunable terahertz pulses via relativistic laser-foil interactions, Phys. Rev. X **10,** 031062 (2020).

[33] J. Fuchs, P. Antici, E. D'Humières, E. Lefebvre, M. Borghesi, E. Brambrink *et al.*, Laser-driven proton scaling laws and new paths towards energy increase, Nat. Phys. **2,** 48 (2006). The ion acceleration time is evaluated as $t_{acc} = \alpha \cdot (\tau_L + 60$ fs), where τ_L is the laser pulse duration, and α varies from 2.5 to 1.9 for the intensity $(1-2) \times 10^{19}$ W/cm^2.

[34] P. Mora, Plasma expansion into a vacuum, Phys. Rev. Lett. **90,** 185002 (2003).